

The Peculiar Type Ic Supernova 1997ef: Another Hypernova

Koichi IWAMOTO¹, Takayoshi NAKAMURA², Ken'ichi NOMOTO^{2,3}, Paolo A. MAZZALI^{3,4},
I. John DANZIGER⁴, Peter GARNAVICH⁵, Robert KIRSHNER⁵, Saurabh JHA⁵,
David BALAM⁶, and John THORSTENSEN⁷

¹ Department of Physics, College of Science and Technology, Nihon University, Chiyoda-ku,
Tokyo 101-8308, Japan

² Department of Astronomy, School of Science, University of Tokyo, Bunkyo-ku, Tokyo 113-0033,
Japan

³ Research Center for the Early Universe, School of Science, University of Tokyo, Bunkyo-ku,
Tokyo 113-0033, Japan

⁴ Osservatorio Astronomico di Trieste, via G.B. Tiepolo 11, I-34131 Trieste, Italy

⁵ Harvard-Smithsonian Center for Astrophysics, 60 Garden Street, Cambridge, MA 02138, USA

⁶ University of Victoria, Victoria, BC, Canada

⁷ Dartmouth College, Department of Physics and Astronomy, Hanover, NH 03755, USA

Received May 26, 1998 (in original form); accepted _____

ABSTRACT

SN 1997ef has been recognized as a peculiar supernova from its light curve and spectral properties. The object was classified as a Type Ic supernova (SN Ic) because its spectra are dominated by broad absorption lines of oxygen and iron, lacking any clear signs of hydrogen or helium line features. The light curve is very different from that of previously known SNe Ic, showing a very broad peak and a slow tail. The strikingly broad line features in the spectra of SN 1997ef, which were also seen in the hypernova SN 1998bw, suggest the interesting possibility that SN 1997ef may also be a hypernova.

The light curve and spectra of SN 1997ef were modeled first with a standard SN Ic model assuming an ordinary kinetic energy of explosion $E_K = 10^{51}$ erg. The explosion of a CO star of mass $M_{\text{CO}} \approx 6M_{\odot}$ gives a reasonably good fit to the light curve but clearly fails to reproduce the broad spectral features. Then, models with larger masses and energies were explored. Both the light curve and the spectra of SN 1997ef are much better reproduced by a C+O star model with $E_K = 8 \times 10^{51}$ erg and $M_{\text{CO}} = 10M_{\odot}$. Therefore, we conclude that SN 1997ef is very likely a hypernova on the basis of its kinetic energy of explosion. Finally, implications for the deviation from spherical symmetry are discussed in an effort to improve the light curve and spectral fits.

Subject headings: gamma rays: bursts — radiation transfer: light curves — radiation transfer: spectra — stars: massive — stars: supernovae — stars: supernovae: individual (SN 1997ef)

1. INTRODUCTION

The supernova 1997ef (SN 1997ef) was discovered on November 25, 1997 at an R magnitude of 16.7 near the spiral galaxy UGC4107 (Sano 1997). The first spectrum was taken on November 26 (Garnavich et al. 1997a). Subsequently, photometric and spectroscopic follow-ups have provided high quality optical light curves and spectra (Garnavich et al. 1997a,b,c; Hu et al. 1997; Filippenko et al. 1997; Wang et al. 1998). As seen in Figure 1, the spectra of SN 1997ef are dominated by broad oxygen and iron lines but do not show any clear feature of hydrogen or helium (Garnavich et al. 1997b; Filippenko et al. 1997), showing the overall similarity to other Type Ic supernovae (SNe Ic). This led us to classify SN 1997ef as a Type Ic supernova.

In Figure 2 the visual light curve of SN 1997ef (Garnavich et al. 1997b,c) is compared with those of SN 1998bw (Galama et al. 1998) and the ordinary SN Ic 1994I (Richmond et al. 1996a,b). Despite the spectral similarity, the light curve of SN 1997ef is quite different from those of SN 1998bw and SN 1994I. It has quite a flat peak, much broader than those of the other SNe Ic. Besides, the tail of the light curve of SN 1997ef starts late and the rate of its decline is much slower than in other SNe Ic. It is also true that light curves are rather diverse, even in this limited number of samples, probably reflecting the differences in energy and progenitor mass of SN Ic explosions.

The most striking and peculiar characteristic of SN 1997ef is the breadth of its line features. Such broad spectral features were later recognized to be a distinguishing property of the spectra in SN 1998bw as well(Figure 1). SN 1998bw was discovered within the error box of GRB980425 determined by the BeppoSAX satellite, only 0.9 days after the date of the gamma-ray burst (GRB), and therefore probably related to this GRB (Galama et al. 1998). The very broad spectra and the light curve shape have led to the conclusion that SN 1998bw had an extremely large kinetic energy of explosion, $E_K \sim 3 \times 10^{52}$ ergs (Iwamoto et al. 1998; Woosley, Eastman, & Schmidt 1999). This is one order of magnitude larger than the energy of typical supernovae, thus SN 1998bw was called a “hypernova” (Iwamoto et al. 1998).

The spectral similarity between SN 1997ef and SN 1998bw suggests the interesting possibility that SN 1997ef may also be a hypernova. In addition, a possible connection with a GRB has been suggested for SN 1997ef: GRB971115 appears to be compatible with the supernova in the position and the time of occurrence (Wang & Wheeler 1998). Since the statistical significance for this case is much weaker than for the case of SN 1998bw and GRB980425, it is difficult to confirm the physical association between SN 1997ef and GRB971115. However, it is possible at least to clarify whether SN 1997ef is a hypernova or not by estimating the kinetic energy of explosion through modeling of light curves and spectra as in the case of SN 1998bw (Iwamoto et al. 1998; Mazzali 1999). In fact, this is exactly the primary purpose of this paper.

We have constructed supernova progenitor models and performed detailed hydrodynamics and radiation transfer calculations to obtain light curves and spectra for the explosion models. The results are compared with observations of SN 1997ef, to derive its explosion energy and the ejecta mass, and thus to determine whether SN 1997ef was an ordinary SN Ic or a hypernova. Since the light curves of the other SNe Ic 1994I and 1998bw were successfully reproduced by the collapse-induced explosion of C+O stars (Nomoto et al. 1994; Iwamoto et al. 1994; Iwamoto et al. 1998), we adopt C+O stars as progenitor models for SN 1997ef as well.

This paper consists of five sections that follow this introduction. Section 2 describes the ordinary SN Ic model and the hypernova model. The method and results of our light curve calculations are presented in §3. The synthetic spectra are compared with the observations in §4. Section 5 is devoted to discussion of various issues including the SN-GRB connection and possible progenitor scenarios. Finally, our conclusions are summarized in §6.

2. EXPLOSION MODELS FOR SUPERNOVAE AND HYPERNOVAE

We constructed hydrodynamical models of an ordinary SN Ic and a hypernova as follows.

(1) For the ordinary SN Ic (model CO60), a C+O star with a mass $M_{\text{CO}} = 6.0M_{\odot}$ (which is the core of a $25 M_{\odot}$ main-sequence star) is exploded with explosion kinetic energy $E_{\text{K}} = 1.0 \times 10^{51}$

ergs and ejecta mass $M_{\text{ej}} = M_{\text{CO}} - M_{\text{rem}} = 4.6M_{\odot}$. Here M_{rem} ($= 1.4 M_{\odot}$) denotes the mass of the compact star remnant (either a neutron star or a black hole).

(2) For the hypernova model (CO100), a C+O star of $M_{\text{CO}} = 10.0M_{\odot}$ is constructed from the $10 M_{\odot}$ He star (which has a $8 M_{\odot}$ C+O core) by replacing He in the outer $2 M_{\odot}$ layer with C+O. This model corresponds to 30 - 35 M_{\odot} on the main-sequence. The progenitor model is exploded with $E_{\text{K}} = 8.0 \times 10^{51}$ ergs and $M_{\text{ej}} = 7.6M_{\odot}$, i.e., $M_{\text{rem}} = 2.4 M_{\odot}$.

The hydrodynamics at early phases were calculated using a Lagrangian PPM code (Colella & Woodward 1984) with a simple nuclear reaction network including 13 elements (Müller 1986). Detailed nucleosynthesis calculations with 240 species (Hix & Thielemann 1996) are carried out as post-processing for each layer. The explosions are simulated by placing the mass cut so that the ^{56}Ni mass is $M(^{56}\text{Ni}) = 0.15M_{\odot}$ and by depositing thermal energy in a few zones just below the mass cut so that the final kinetic energy is the selected value.

The above values of M_{rem} are determined in this way to reproduce the maximum brightness of SN 1997ef by the radioactive decays with $M(^{56}\text{Ni}) = 0.15M_{\odot}$. The compact star in CO60 is a neutron star because $M_{\text{rem}} = 1.4 M_{\odot}$, while it may be a black hole in CO100 because M_{rem} ($= 2.4 M_{\odot}$) may well exceed the maximum mass of a neutron star.

These model parameters are summarized in Table 1 and can be constrained by comparing the calculated light curves and synthetic spectra. For comparison, the parameters of models CO21 for SN 1994I (Nomoto et al. 1994; Iwamoto et al. 1994) and CO138 for SN 1998bw (Iwamoto et al. 1998; Nakamura et al. 1999a) are also given in Table 1. We constructed the progenitor model by attaching a thin hydrostatic and thermal-equilibrium C+O envelope to the C+O core of the presupernova model (Nomoto & Hashimoto 1988; Hashimoto 1995).

The expansion soon becomes homologous, so that $v \propto r$. The solid lines in Figure 3 show the density-velocity distributions of the homologously expanding ejecta at $t = 16$ days for CO60 and CO100. The dashed line shows the modified structure for the spectrum calculation as will be discussed in §4. The expansion velocities are clearly higher in CO100 than in CO60. Figures 4 and

5 show the composition structure for models CO60 and CO100, respectively, against the expansion velocities and the Lagrangian mass coordinate of the progenitor. In CO100, the Fe and Si-rich layers expand much faster than in CO60. The total nucleosynthesis products are summarized in Table 2.

3. LIGHT CURVE MODELS

3.1. Radiation Hydrodynamics Code

The light curve calculation is started, when the ejecta has reached the homologous expansion phase, with a one-dimensional spherically symmetric radiation transfer code (Iwamoto 1997).

The code solves the multi-frequency radiative transfer equation for the specific intensity I_ν in the comoving frame, including all terms up to the first order in v/c (Mihalas & Mihalas 1984),

$$\begin{aligned}
 \frac{1}{c} \frac{\partial I_\nu}{\partial t} + \frac{\mu}{r^2} \frac{\partial}{\partial r} (r^2 I_\nu) &+ \frac{\partial}{\partial \mu} \left\{ (1 - \mu^2) \left[\frac{1}{r} + \frac{\mu}{c} \left(\frac{v}{r} - \frac{\partial v}{\partial r} \right) \right] I_\nu \right\} \\
 &- \frac{\partial}{\partial \nu} \left\{ \nu \left[(1 - \mu^2) \frac{v}{cr} + \frac{\mu^2}{c} \frac{\partial v}{\partial r} \right] I_\nu \right\} \\
 &+ \left[(3 - \mu^2) \frac{v}{cr} + \frac{1 + \mu^2}{c} \frac{\partial v}{\partial r} \right] I_\nu \\
 &= \kappa_\nu B_\nu - \kappa_\nu I_\nu - \sigma_\nu I_\nu + \frac{1}{4\pi} \int \sigma_\nu I_\nu d\Omega, \tag{1}
 \end{aligned}$$

where κ_ν and σ_ν are the absorptive and scattering opacities, respectively, B_ν is the Planck function and μ is the cosine of the angle made by the radial direction and the direction of the ray. This equation is solved numerically using the Feautrier method with an approximate Lambda operator similar to the one described by Hauschildt (1992).

To determine the gas temperatures, Equation (1) is solved simultaneously with the energy equation and the first two moment equations of Equation (1). The energy equation of the radiation plus gas is written as

$$\frac{\partial}{\partial t} \left(e + \frac{E}{\rho} \right) = \epsilon - (P + fE) \frac{\partial}{\partial t} \left(\frac{1}{\rho} \right) - 4\pi \frac{\partial}{\partial M_r} (r^2 F) + (3f - 1) \frac{vE}{\rho r}, \quad (2)$$

while the radiation energy and momentum equations are

$$\frac{\partial}{\partial t} \left(\frac{E}{\rho} \right) = \frac{c}{\rho} (\kappa_P a T^4 - \kappa_E E) - fE \frac{\partial}{\partial t} \left(\frac{1}{\rho} \right) - 4\pi \frac{\partial}{\partial M_r} (r^2 F) + (3f - 1) \frac{vE}{\rho r}, \quad (3)$$

and

$$\frac{\partial F}{\partial t} = - \left(c\chi_F + \frac{2v}{r} \right) F - 4\pi r^2 \rho \left(c^2 \frac{\partial(fE)}{\partial M_r} + 2F \frac{\partial v}{\partial M_r} \right) - (3f - 1) \frac{c^2 E}{r}, \quad (4)$$

respectively, where e is the thermal energy of the ions and electrons per unit mass, and E , F and f are the radiation energy density, flux, and the Eddington factor defined below:

$$E = \frac{2\pi}{c} \int_0^\infty d\nu \int_{-1}^1 I_\nu d\mu, \quad (5)$$

$$F = 2\pi \int_0^\infty d\nu \int_{-1}^1 I_\nu \mu d\mu, \quad (6)$$

$$f = \frac{\int_0^\infty d\nu \int_{-1}^1 I_\nu \mu^2 d\mu}{\int_0^\infty d\nu \int_{-1}^1 I_\nu d\mu}. \quad (7)$$

Partial derivatives with respect to t in Equations (1)-(4) are all Lagrangian time derivatives.

The absorptive and scattering parts of the opacity are given as

$$\kappa_\nu = \epsilon(\kappa_{b-b} + \kappa_{b-f}) + \kappa_{f-f}, \quad (8)$$

and

$$\sigma_\nu = (1 - \epsilon)(\kappa_{b-b} + \kappa_{b-f}) + n_e \sigma_T, \quad (9)$$

κ_{b-b} , κ_{b-f} and κ_{f-f} are the bound-bound, bound-free, and free-free opacities, respectively; n_e is the number density of free electrons, and σ_T is the Thomson scattering cross section. In the moment equations, the energy mean (κ_E) and the Planck mean opacities (κ_P) include only the absorptive part, while the flux mean opacity (χ_F) is the total opacity. For bound-bound transitions, energy levels and transition probabilities are taken from the compilation by Kurucz (1991). For bound-free data, we use the analytic fitting formula to the photoionization cross sections given by Verner & Yakovlev (1995). Local Thermodynamic Equilibrium (LTE) is assumed

to determine the ionization balance and the level populations of each ion. However, the non-LTE effect is taken into account approximately by assuming that the value of the absorptive fraction ϵ is a constant less than unity in Equations (8) and (9). Experiments of spectral syntheses have shown that a value $\epsilon = 0.1$ is a reasonable choice for this fraction (Baron et al. 1996).

The energy deposition due to the radioactive decays is calculated with a one energy-group γ -ray-transfer code. We assume an absorptive opacity $\kappa_\gamma = 0.03$ and the complete trapping of positrons. The rest-frame flux is calculated from the comoving-frame intensities using the following transformation:

$$F_{\nu,\text{rest}} = 2\pi \int_{-1}^1 (\mu + \beta) I \left(\mu, \frac{\nu}{1 + \beta\mu} \right) d\mu, \quad (10)$$

$$F_{\lambda,\text{rest}} = \frac{\nu^2}{c} F_{\nu,\text{rest}}. \quad (11)$$

For the calculation of the light curves of CO60 and CO100 discussed in the next subsection, we use 200 radial mesh points to solve the moment Equations (2)-(4), while 800 frequency and 50 radial mesh points were used for the multi-frequency radiative transfer Equation (1).

3.2. Light Curve Models

In Figure 6 we compare the synthetic V light curves for models CO60 and CO100 with the observed V light curve of SN1997ef. We adopt a distance of 52.3 Mpc (a distance modulus of $\mu = 33.6$ mag) as estimated from the recession velocity, $3,400 \text{ km s}^{-1}$ (Garnavich et al. 1997a) and a Hubble constant $H_0 = 65 \text{ km s}^{-1} \text{ Mpc}^{-1}$. We assume no color excess ($E(B - V) = 0.00$); this is justified by the fact that no signature of a narrow Na I D interstellar absorption line is visible in the spectra of SN 1997ef at any epoch (Garnavich 1997a).

The light curve of SN 1997ef has a very broad maximum, which lasted for ~ 25 days. This is much broader than in both the ordinary SN Ic 1994I and the hypernova SN 1998bw. The light curve tail of SN 1997ef starts only ~ 40 days after maximum, much later than in other SNe Ic.

The slow light curve of SN 1997ef can be reproduced with different explosion models. The properties of these models are constrained by the fact that the peak width, τ_{LC} , which reflects the time scales of photon diffusion and hydrodynamical expansion, scales approximately as

$$\tau_{\text{LC}} \propto \kappa^{1/2} M_{\text{ej}}^{3/4} E_{\text{K}}^{-1/4}, \quad (12)$$

where κ denotes the optical opacity (Arnett 1996). Since the model parameters of C100 and CO60 give similar τ_{LC} , the synthetic light curves of the two models look similar: both have quite a broad peak and reproduce the light curve of SN1997ef reasonably well (Fig. 6).

The light curve shape depends also on the distribution of ^{56}Ni , which is produced in the deepest layers of the ejecta. More extensive mixing of ^{56}Ni leads to an earlier rise of the light curve to the peak. For SN 1997ef, the best fit is obtained when the ^{56}Ni is mixed almost uniformly to the surface for both models. Without mixing of ^{56}Ni , the rising time to $V = 16.5$ mag is ~ 30 d for CO100, which is clearly too long to be compatible with the spectroscopic dating (see §4).

Model CO60 has the same kinetic energy ($E_{\text{K}} = 1 \times 10^{51}$ erg) as model CO21, which was used for SN Ic 1994I (see Table 1 for the model parameters). In order to reproduce the light curve of SN 1997ef, which is much slower than that of SN 1994I, therefore, the ejecta mass of CO60 is ~ 5 times larger than that of CO21.

The ejecta mass of CO100 is a factor of ~ 2 larger than that of CO60, and it is only $\sim 20\%$ smaller than that of model CO138, which was used for SN 1998bw (Table 1). Thus the explosion energy of CO100 is ~ 8 times larger than that of CO60 to reproduce SN 1997ef. This is very energetic, but still it is much smaller than the explosion energy of CO138. The smaller E_{K} for a comparable mass allows CO100 to reproduce the light curve of SN 1997ef, which has a much broader peak than that of SN 1998bw.

SN 1997ef entered the light curve tail around day 40. Afterwards, the observed V-light curve declined at a rate of $\sim 1.1 \times 10^{-2}$ mag day $^{-1}$, which is slower than in other SNe Ic and is actually close to the ^{56}Co decay rate 9.6×10^{-3} mag day $^{-1}$. Such a slow decline implies much more efficient γ -ray trapping in the ejecta of SN 1997ef than in SN 1994I. The ejecta of both CO100 and CO60

are fairly massive and trap a large fraction of the γ -rays, so that the calculated light curves have slower tails compared with CO21.

However, the calculated light curves of both models decline somewhat faster than the observed tail. A similar discrepancy has been noted for the Type Ib supernovae (SNe Ib) 1984L and 1985F (Swartz & Wheeler 1991; Baron, Young, & Branch 1993). The late time light curve decline of these SNe Ib is as slow as the ^{56}Co decay rate, so that the inferred value of M is significantly larger (and/or E_K is smaller) compared with those obtained from fitting the early light curve shape. Baron et al. (1993) suggested that the ejecta of these SNe Ib must be highly energetic and as massive as $\sim 50 M_\odot$. In §5.2, we will suggest that such a discrepancy between the early and late light curves might be an indication of some aspherical effects in SN 1997ef and possibly in SNe Ib as well.

As we have shown, light curve modeling provides important constraints on M_{CO} and E_K . However, it is difficult to distinguish between the ordinary SN Ic and the hypernova model from the light curve alone, since models with different values of M_{ej} and E_K can reproduce the observed light curve almost equally well. On the other hand, these models can be expected to show different evolution of the photospheric velocities and spectra as will be discussed in the following sections.

3.3. Photospheric Velocities

The photospheric velocity roughly scales as $v \propto M_{\text{ej}}^{-1/2} E_K^{1/2}$, so that M_{ej} and E_K can be constrained in a different way from the light curve width. Figure 7 shows the evolution of the observed velocities of the Si II line measured in the spectra at the absorption core and the velocities at the photosphere computed from models CO60 and CO100. The velocity of the Si II line is somewhat larger than that of the photosphere, and at the earliest time it reaches $\sim 20,000$ km s $^{-1}$. For CO60 the photosphere forms at velocities much smaller than those of the observed lines, while CO100 gives photospheric velocities sufficiently high to be regarded as consistent with the observations. The apparent discrepancy between the model and observations at the earliest

phase may be related to the outer density structure as will be discussed in §4.

This comparison appears to favor the hyper-energetic model CO100 over the ordinary model CO60. At later phases, however, the Si II velocities decrease faster than the calculated photospheric velocities. We examine this problem with synthetic spectra in §4.

4. SYNTHETIC SPECTRA

As discussed in the earlier sections, it is difficult to distinguish between the models based only on their light curves. On the other hand, this can be done with spectrum synthesis, because the different densities and photospheric velocities lead to different spectra.

Around maximum light, the spectra of SN 1997ef show just a few very broad features, and are quite different from those of ordinary SNe Ib/c, but similar to SN 1998bw. However, at later epochs the spectra develop features that are easy to identify, such as the Ca II IR triplet at $\sim 8200\text{\AA}$, the O I absorption at 7500\AA , several Fe II features in the blue, and they look very similar to the spectrum of the ordinary SN Ic 1994I.

We computed synthetic spectra with a Monte Carlo spectrum synthesis code using the density structure and composition of the hydrodynamic models CO60 and CO100. The code is based on the pure scattering code described by Mazzali & Lucy (1993), but has been improved to include photon branching, so that the reprocessing of the radiation from the blue to the red is followed more accurately and efficiently (Lucy 1999; Mazzali 1999).

We produced synthetic spectra for six epochs representative of the evolution of SN 1997ef: Nov 29, Dec 5, and Dec 17, which are all around maximum, Dec 24 and Jan 1, at the beginning of the decline phase, and Jan 26, which is already on the tail of the light curve. As in the light curve comparison, we adopted a distance modulus of $\mu = 33.6$ mag, and $E(B - V) = 0.00$. The model parameters, the computed temperatures and the magnitudes of the synthetic spectra for CO100 are listed in Table 3.

In Figure 8 we show the synthetic spectra computed with the ordinary SN Ic model CO60 for the first three epochs, where the spectra are most sensitive to differences in mass and kinetic energy. The lines in the spectra computed with this model are always much narrower than the observations. This clearly indicates a lack of material at high velocity in model CO60, and suggests that the kinetic energy of this model is much too small.

Synthetic spectra obtained with the hypernova model CO100 for the same 3 epochs are shown in Figure 9. The spectra show much broader lines, and are in better agreement with the observations. In particular, the blending of the Fe lines in the blue, giving rise to broad absorption troughs, is well reproduced, and as is the very broad Ca-O feature in the red particularly for the 5 Dec spectrum. The two ‘emission peaks’ observed at ~ 4400 and 5200\AA correspond to the only two regions in the blue that are relatively line-free. A similar situation is observed in SN 1998bw (Iwamoto et al. 1998).

The spectra are characterized by a low temperature, even near maximum, because the rapid expansion combined with the relatively low luminosity (from the tail of the light curve we deduce that SN 1997ef produced about $0.15M_{\odot}$ of ^{56}Ni , compared to about $0.6M_{\odot}$ in a typical SN Ia and $0.7M_{\odot}$ in SN 1998bw) leads to rapid cooling. Thus the SiIII 6355\AA line is not very strong.

Although model CO100 yields rather good synthetic spectra, it still fails to reproduce the observed large width of the O I - Ca II feature in the only near-maximum spectrum that extends sufficiently far to the red (5 Dec 1997). An improvement can be obtained by introducing an arbitrary flattening of the density profile at the highest velocities. The original model has an outer density dependence $\rho \sim r^{-8}$ (the solid line in Fig. 3), but we found that a density law $\rho \sim r^{-4}$ for $v > 25,000 \text{ km s}^{-1}$ (shown as the dotted line in Fig. 3) gives rise to significant absorption at $v \sim 30,000 - 40,000 \text{ km s}^{-1}$, yielding spectra where the required blending is achieved. These are shown as the dotted lines in Figure 9.

In the synthetic spectra computed for the following 3 epochs, all absorptions are deeper, which is a consequence of the photosphere receding inside the ejecta. The original model CO100 does not have material at velocities smaller than $\sim 5,000 \text{ km s}^{-1}$ (Fig. 3, solid line). Therefore,

the density distribution has to be modified to extend to lower velocities, as indicated by the dotted line in Figure 3 (see discussion in §5.1). The spectra computed with this modified model CO100 reproduce the observations reasonably well, but display narrower features than the observed spectra. Although at these late epochs it is not so easy to distinguish among different explosion models, this discrepancy suggests that a density structure with an even flatter profile between 3,000 and 10,000 km s⁻¹ could yield better synthetic spectra.

Full details of the spectrum synthesis calculations, including insights on the density structure and the abundance in the ejecta will be given in a separate paper (Mazzali et al., 1999, in preparation).

5. DISCUSSION

5.1. Possible Aspherical Effects

We have shown that the light curve, the photospheric velocities, and the spectra of SN 1997ef are much better reproduced with the hyper-energetic model CO100 than with the ordinary SN Ic model CO60. However, there remain several features which are difficult to explain with the present models. Such features were seen at late times, and might indicate some aspherical effects, as discussed below.

(1) The synthetic spectra are in good agreement with observations until day 50 (Fig. 9). However, in order to obtain a reasonably good agreement with the observed spectrum at day 50, the photospheric velocity must be as low as $\sim 3,000$ km s⁻¹. Then the density structure needs to be modified to increase towards the central, low velocity region, compared with the density structure in the original model (Fig. 3).

(2) The velocity of Si II, which is as high as $\sim 30,000$ km s⁻¹ at the earliest phase, also decreases to as low as $\sim 3,000$ km s⁻¹ around day 50 (Fig. 7). Such low velocity Si also suggests the presence of a low velocity core as indicated by the synthetic spectrum.

(3) Despite the good agreement between the calculated and observed light curves near maximum, the calculated light curve tail declines faster than the observations (Fig. 6). This deviation implies that a larger fraction of the γ -rays must be trapped in the ejecta than in CO100. This also suggests that there might be a high density region in the ejecta of SN1997ef, where the γ -rays deposit most easily.

(4) Extensive mixing of ^{56}Ni is required to reproduce the rise time of the light curve. In addition, spectral fits do not seem to suggest that the Fe abundance increases in deeper layers. According to hydrodynamical simulations of the ‘Rayleigh-Taylor instability in the ejecta of envelope-stripped supernovae (Hachisu et al. 1991; Iwamoto et al. 1996), large scale mixing is not expected to occur in massive progenitors because the density gradient is not steep enough around the composition interfaces. One possibility to induce such mixing in the velocity space is an asymmetric explosion. Higher velocity ^{56}Ni reaches the ejecta surface and the effect of radioactive heating comes up as early as is required from light curve modeling.

In order to realize higher densities at low velocity regions without increasing the mass of ejecta significantly, the explosion may be required to be spherical. If the explosion is somewhat aspherical, the shock would be stronger and the material would expand at a larger velocity in a certain direction, while in the perpendicular directions, on the other hand, the shock would be weaker, ejecting slower velocity material. The density of the central region could be high enough for γ -rays to be trapped even at advanced phases, thus giving rise to a slowly declining tail (see Nakamura et al. 1999a for a discussion of SN 1998bw). In the extremely asymmetric cases, the material ejection may happen in a jet-like form. A jet could easily bring some ^{56}Ni from the deepest layer to the surface of high velocities. Detailed spectral analysis of observed spectra for different epochs are necessary to investigate this issue further.

5.2. Gamma-Ray Bursts/Supernovae Connection and SN 1997ef

There have been an increasing number of candidates for the gamma-ray burst (GRB)/supernova connection, including GRB980425/SN1998bw (Galama et al. 1998; Iwamoto et al. 1998; Iwamoto 1999), GRB970514/SN1997cy (Germany et al. 1999; Turatto et al. 1999), GRB980910/SN1999E (Thorsett & Hogg 1999). Two other high- z GRBs may also be associated with a supernova: GRB980326 (Bloom et al. 1999) and GRB970228 (Reichart 1999; Galama et al. 1999). The optical transients of these GRBs showed significant reddening and temporal slow down (even with a second maximum) in their late light curves, which can be fitted by the early power law decay plus the red-shifted light curve of SN 1998bw.

As noted in §1, a possible connection between SN 1997ef and GRB971115 has been suggested (Wang & Wheeler 1998). Recently another SN Ic, 1998ey, showed a spectrum with very broad features, very similar spectra to that of SN1997ef on Dec 17 (Garnavich et al. 1998); but no GRB counterpart has been proposed for SN 1998ey. Although this may cast some doubt on the general association between hypernovae and GRBs, it must be noted that both SNe 1997ef and 1998ey were less energetic events than SN 1998bw. It is possible that a weaker explosion is less efficient in collimating the γ -rays to give rise to a detectable GRB (GRB980425 was already quite weak compared to the average GRBs), or that orientation somewhat away from the beam axis results in a seemingly weaker supernova and in the non-detection of the GRB. Only the accumulation of more data will allow us to address these questions.

5.3. The Mass of Ejected ^{56}Ni

For the study of the chemical evolution of galaxies, it is important to know the mass of ^{56}Ni , $M(^{56}\text{Ni})$, synthesized in core-collapse supernovae as a function of the main-sequence mass M_{ms} of the progenitor star (e.g., Nakamura et al. 1999b). From our analysis of SN 1997ef, we can add a new point to this relation.

We evaluate the uncertainty in our estimates of $M(^{56}\text{Ni})$ and M_{ms} . We need $0.15 M_{\odot}$ of ^{56}Ni

to get a reasonable fit to the light curve of SN 1997ef at a distance $D = 52.3$ Mpc. The expected 10% uncertainty in the distance leads to a 20% uncertainty in the ^{56}Ni mass, i.e., $M(^{56}\text{Ni}) = 0.15 \pm 0.03 M_{\odot}$. The distribution of ^{56}Ni affects the peak luminosity somewhat, but the effect is found to be much smaller than that of the uncertainty in the distance. A $10 M_{\odot}$ C+O star corresponds to a $M_{\text{ms}} = 30 - 35 M_{\odot}$, but the uncertainty involved in the conversion of the core mass to M_{ms} may involve a larger uncertainty if the progenitor undergoes close binary evolution.

Figure 10 shows a plot of $M(^{56}\text{Ni})$ against M_{ms} , both of which are obtained from fitting the optical light curves of SNe 1987A, 1993J, and 1994I (e.g., Shigeyama & Nomoto 1990; Nomoto et al. 1993, 1994; Shigeyama et al. 1994; Iwamoto et al. 1994; Woosley et al. 1994; Young, Baron, & Branch 1995). The amount of ^{56}Ni appears to increase with increasing M_{ms} of the progenitor, except for SN II 1997D (Turatto et al. 1998).

We interpret this relation as follows. Stars with $M_{\text{ms}} \lesssim 25 M_{\odot}$ form a neutron star, producing $\sim 0.08 \pm 0.03 M_{\odot}$ ^{56}Ni as in SN I Ib 1993J, SN Ic 1994I, and SN 1987A (although SN 1987A may be a borderline case between neutron star and black hole formation). Stars with $M_{\text{ms}} \gtrsim 25 M_{\odot}$ form a black hole (e.g., Ergma & van den Heuvel 1998); whether they become hypernovae or ordinary SNe II may depend on the angular momentum in the collapsing core. For SN 1997D, because of the large gravitational potential, the explosion energy is so small that most of ^{56}Ni fell back onto a compact star remnant; the fall-back might cause a collapse of the neutron star into a black hole. The core of SN II 1997D might not have much angular momentum, because the progenitor had a massive H-rich envelope so that the angular momentum of the core might have been transported to the envelope via a magnetic field effect. Similarly, negligible ejection of ^{56}Ni in black hole formation has recently been suggested for X-ray Nova Sco (GRO J1655-40), where the companion star of the black hole seems to be enriched with S, Si, Mg, and O but not Fe (Israelian et al. 1999). Hypernovae such as SNe 1998bw, 1997ef, and 1997cy might have rapidly rotating cores owing possibly to the spiraling-in of a companion star in a binary system. The outcome certainly depends also on mass loss and binarity.

As noted in §5.2, it has been claimed that the optical afterglows of GRB's 980326 and 970228

are better reproduced if the red-shifted light curve of SN 1998bw is added to the power-law light curve (Bloom et al. 1999; Reichart 1999; Galama et al. 1999). A question arising from these two examples is whether the supernovae associated with GRBs have a similar maximum luminosity, i.e., whether $0.7 M_{\odot}$ ^{56}Ni production as in SN 1998bw is rather common. However, the present study of SN 1997ef shows that the ^{56}Ni mass and thus intrinsic maximum brightness is smaller than in SN 1998bw by a factor of 4 - 5 (see the next subsection). We certainly need more examples for defining the actual distribution of masses of ^{56}Ni produced in supernovae/hypernovae.

5.4. Possible Evolutionary Scenarios

Here we classify possible evolutionary paths leading to C+O star progenitors. In particular, we explore the paths to the progenitors that have rapidly rotating cores, because the explosion energy of hypernovae may be extracted from rapidly rotating black holes.

(1) Case of a single star: If the star is as massive as $M_{\text{ms}} \gtrsim 40 M_{\odot}$, it could lose H and He envelopes in a strong stellar wind (e.g., Schaller et al. 1992). This would be a Wolf-Rayet star.

(2) Case of a close binary system: Suppose we have a close binary system with a large mass ratio. In this case, the mass transfer from star 1 to star 2 inevitably takes place in a non-conservative way, and the system experiences a common envelope phase where star 2 is spiraling into the envelope of star 1. If the spiral-in releases enough energy to remove the common envelope, we are left with a bare He star (star 1) and a main-sequence star (star 2), with a reduced separation. If the orbital energy is too small to eject the common envelope, the two stars merge to form a single star (e.g., van den Heuvel 1994).

(2-1) For the non-merging case, possible channels from the He stars to the C+O stars are as follows (Nomoto, Iwamoto, & Suzuki 1995).

(a) Small-mass He stars tend to have large radii, so that they can fill their Roche lobes more easily and lose most of their He envelope via Roche lobe overflow.

(b) On the other hand, larger-mass He stars have radii too small to fill their Roche lobes. However, such stars have large enough luminosities to drive strong winds to remove most of the He layer (e.g., Woosley, Langer, & Weaver 1995). Such a mass-losing He star is observed as a Wolf-Rayet star.

Thus, from a non-merging scenario, we expect two different kinds of SNe Ic, fast and slow, depending on the mass of the progenitor. SNe Ic from smaller mass progenitors (channel a) show a faster light curve and spectral evolution, because the ejecta become more quickly transparent to both gamma-rays and optical photons. The slow SNe Ic originate from the Wolf-Rayet progenitors (channels b and 1). The presence of both slow and fast SNe Ib/Ic has been noted by Clocchiatti & Wheeler (1997).

(2-2) For merging case, the merged star has a large angular momentum, so that its collapsing core must be rapidly rotating. It would lead to the formation of a rapidly rotating black hole from which possibly a hyper-energetic jet could emerge. If the merging process is slow enough to eject H and He envelopes, the star would become a rapidly rotating C+O star. Such C+O stars are the candidates for the progenitors of Type Ic hypernovae like SNe 1997ef and 1998bw. If a significant amount of H-rich (or He) envelope remains after merging, the rapidly rotating core leads to a hypernova of Type IIn possibly like SN 1997cy (or Type Ib).

6. CONCLUSIONS

We have shown that the light curve, the photospheric velocities, and the spectra of SN 1997ef are much better reproduced by the hyper-energetic model CO100 than they are by the ordinary SN Ic model CO60. The model parameters of CO100 are $E_K = 8 \times 10^{51}$ erg, $M_{CO} = 10M_\odot$ (which corresponds to the C+O core of a 30–35 M_\odot star), and $M(^{56}\text{Ni}) = 0.15 M_\odot$. The compact star remnant of CO100 is as massive as $\sim 2.4 M_\odot$, thus possibly being a black hole. The estimated high explosion energy would be extracted from the rapidly rotating black hole.

Compared with SN 1998bw, M_{CO} , $M(^{56}\text{Ni})$ and E_K are all slightly smaller, but SN 1997ef can

certainly be regarded as a *hypernova* in terms of the kinetic energy of the explosion. Therefore, we suggest that SNe 1997ef, 1998ey, and 1998bw form a new class of hyper-energetic Type Ic supernovae, which we call hypernovae. They are distinguished by their large kinetic energy, 8 - 60 times large than in ordinary supernovae.

Despite the hyper-energetic features at early phases of SN 1997ef, the spectra at advanced phases and the slowly declining light curve tail suggest the presence of a low-velocity, relatively dense core, which is not predicted by the high energy spherical models. This discrepancy, as well as the suggested extensive mixing of ^{56}Ni , may indicate that the explosion of SN 1997ef was somewhat aspherical.

This work was started at the Institute for Theoretical Physics, University of California, Santa Barbara, USA, supported under NSF grant no. PHY74-07194. We would like to thank Hideyuki Umeda, David Branch, and Nobert Langer for informative and stimulating discussion. This work has been supported in part by the grant-in-Aid for Scientific Research (05242102, 06233101) and COE research (07CE2002) of the Ministry of Education, Science, and Culture in Japan, and the fellowship of the Japan Society for the Promotion of Science for Japanese Junior Scientists (6728). A part of the computation was carried out on a Fujitsu VPP-500 computer at the Institute of Physical and Chemical Research (RIKEN) and at the Institute of Space and Astronautical Science (ISAS), and on Fujitsu VPP-300 at the National Astronomical Observatory of Japan (NAO, Tokyo).

REFERENCES

- Arnett, W.D. 1996, *Supernovae and Nucleosynthesis* (Princeton University Press)
- Baron, E., Hauschildt, P.H., Nugent, P., & Branch, D. 1996, *MNRAS*, 283, 297
- Baron, E., Young, T.R., & Branch, D. 1993, *ApJ*, 409, 417
- Bloom, J.S. et al. 1999, *Nature*, 401, 453
- Clocchiatti, A., & Wheeler, J. C. 1997, *ApJ*, 491, 375
- Colella, P., & Woodward, P. R. 1984, *J.Comp.Phys.*, 54, 174
- Ergma, E., & van den Heuvel, E.P.J. 1998, *A&A*, 331, L29
- Filippenko, A. V. 1997, *IAU Circ. No.6783*
- Galama, T.J. et al. 1998, *Nature*, 395, 670
- Galama, T.J. et al. 1999, *ApJ*, submitted
- Garnavich, P., Jha, S., Kirshner, R., & Challis, P. 1997a, *IAU Circ. No.6778*
- Garnavich, P., Jha, S., Kirshner, R., Challis, P., & Balam, D. 1997b, *IAU Circ. No.6786*
- Garnavich, P., Jha, S., Kirshner, R., & Challis, P. 1997c, *IAU Circ. No.6798*
- Garnavich, P., Jha, S., & Kirshner, R. 1998, *IAU Circ. No. 7066*
- Germany, L. et al. 1999, *ApJ*, submitted
- Hachisu, I., Matsuda, T., Nomoto, K., & Shigeyama, T. 1991, *ApJ*, 368, L27
- Hauschildt, P.H. 1992, *JQSRT*, 47, 433
- Hix, W.R. & Thielemann, F.-K. 1996, *ApJ*, 460, 869
- Hu, J. Y., Qiu, Y. L., Qiao, Q. Y., & Wei, J. Y. 1997, *IAU Circ. No.6783*

- Israelian, G., Rebolo, R., Basri, G., Casares, J., & Martin, E.L. 1999, *Nature*, 401, 142
- Iwamoto, K. 1997, Ph.D. Thesis, University of Tokyo
- Iwamoto, K. 1999, *ApJ*, 512, L47
- Iwamoto, K., Mazzali, P.A., Nomoto, K., et al. 1998, *Nature*, 395, 672
- Iwamoto, K., Nomoto, K., Höflich, P., Yamaoka, H., Kumagai, S., & Shigeyama, T. 1994, *ApJ*, 437, L115
- Iwamoto, K., Young, T.R., Nakasato, N., Shigeyama, T., Nomoto, K., Hachisu, I., & Saio, H. 1997, *ApJ*, 477, 865
- Kurucz, R. L. 1991, in *Stellar Atmospheres: Beyond Classical Models*, ed. L.Crivellari, I.Hubeny, & D.G.Hummer (Dordrecht: Kluwer), 441
- Lucy, L.B. 1999, *A&A*, in press
- Mazzali, A. P. 1999, *A&A*, submitted
- Mazzali, A. P., & Lucy, L. B. 1993, *A&A*, 279, 447
- Mihalas, D., & Mihalas, B. W. 1984, *Foundation of Radiation Hydrodynamics*, (Oxford Univ. Press)
- Müller, E. 1986, *A&A*, 162, 103
- Nakamura, T., Mazzali, P.A., Nomoto, K., Iwamoto, K., & Umeda, H. 1999a, *Astron. Nachrichten*, in press
- Nakamura, T., Umeda, H., Nomoto, K., Thielemann, F.-K., & Burrows, A. 1999b, *ApJ*, 517, 193
- Nomoto, K., & Hashimoto, M. 1988, *Phys. Rep.*, 163, 13
- Nomoto, K., Iwamoto, K., & Suzuki, T. 1995, *Phys. Rep.*, 256, 173

- Nomoto, K., Suzuki, T., Shigeyama, T., Kumagai, S., Yamaoka, H., & Saio, H. 1993, *Nature*, 364, 507
- Nomoto, K., Yamaoka, H., Pols, O. R., van den Heuvel, E. P. J., Iwamoto, K., Kumagai, S., & Shigeyama, T. 1994, *Nature*, 371, 227
- Reichart, D.E. 1999, *ApJ*, 521, L111
- Richmond, M. W., et al. 1996a, *AJ*, 111, 327
- Richmond, M. W., Treffers, R. R., Filippenko, A. V., & Paik, Y. 1996b, *AJ*, 112, 732
- Sano, S. 1997, *IAU Circ. No.6778*
- Schaller, G., Schaerer, D., Meynet, G., & Maeder, A. 1992, *A&AS*, 96, 269
- Shigeyama, T., & Nomoto, K. 1990, *ApJ*, 360, 242
- Shigeyama, T., Suzuki, T., Kumagai, S., Nomoto, K., Saio, H., & Yamaoka, H. 1994, *ApJ*, 420, 341
- Swartz, D. A., & Wheeler, J. C. 1991, *ApJ*, 379, L13
- Thorsett, S.E. & Hogg, D.W. 1999, *GCN Cir. No.197*
- Turatto, M., Mazzali, P. A., Young, T. R., Nomoto, K., Iwamoto, K., Benetti, S., Cappellaro, E., Danziger, I. J., de Mello, D. F., Phillips, M. M., Suntzeff, N. B., Clocchiatti, A., Piemonte, A., Leibundgut, B., Covarrubias, R., Maza, J., Sollerman, J., 1998, *ApJ*, 498, L129
- Turatto, M., Suzuki, T., et al. 1999, *ApJ*, submitted
- van den Heuvel, E. P. J. 1994, in *Interacting Binaries*, ed. H. Nussbaumer & A.Orr (Berlin:Springer Verlag), 263
- Verner, D. A., & Yakovlev, D. G. 1995, *A&AS*, 109, 125

Wang, L., & Wheeler, J. C. 1998, ApJ, 504, L87

Woosley, S. E., Eastman, R. G., & Schmidt, B.P. 1999, ApJ, 516, 788

Woosley, S. E., Eastman, R. G., Weaver, T. A., & Pinto, P. A. 1994, ApJ, 429, 300

Woosley, S. E., Langer, N., & Weaver, T. A. 1995, ApJ, 448, 315

Young, T., Baron, E., & Branch, D, 1995, ApJ, 449, L51

Table 1. Parameters of the CO star models

model	C+O core mass (M_{\odot})	ejecta mass (M_{\odot})	^{56}Ni mass (M_{\odot})	E_K (10^{51} erg)
CO21	2.1	0.9	0.07	1
CO60	6.0	4.4	0.15	1
CO100	10.0	7.6	0.15	8
CO138	13.8	10.8	0.7	~ 30

Table 2. The predicted yields of SN1997ef (M_{\odot})

model	C	O	Si	S	Ca	Fe
CO60	5.2×10^{-2}	3.0	0.10	3.7×10^{-2}	5.7×10^{-3}	0.16
CO100	0.58	5.6	0.42	0.19	2.5×10^{-2}	0.19

model	^{44}Ti	^{56}Ni	^{57}Ni
CO60	2.1×10^{-4}	0.15	5.7×10^{-3}
CO100	4.5×10^{-5}	0.15	5.7×10^{-3}

Table 3. Parameters of the synthetic spectra

date	epoch	L	v_{ph}	v_{SiII}	$\log \rho_{ph}$	Mass	T_{eff}	T_{bb}	B_{mod}	V_{mod}	V_{obs}	BC	M_{mod}
	days	erg s $^{-1}$	km s $^{-1}$	R_{\odot}	g cm $^{-3}$	M_{\odot}	K	K					
29 Nov	9	42.17	15500	19072	-12.65	0.71	6123	7666	17.45	16.75	16.7	0.28	-16.700
5 Dec	15	42.19	9500	13962	-12.30	3.02	6128	9407	17.35	16.63	16.5	0.35	-16.750
17 Dec	27	42.24	7500	8011	-12.67	4.79	5291	6697	17.70	16.59	16.6	0.26	-16.875
24 Dec	34	42.17	4900	5378	-12.71	7.29	5602	7529	17.84	16.73	16.8	0.30	-16.700
1 Jan	42	42.03	3600	3775	-12.78	8.32	5426	6904	18.38	17.21	17.3	0.16	-16.350
26 Jan	67	41.84	1950	–	-13.23	9.07	5232	5793	19.10	17.77	18.0	0.08	-15.875

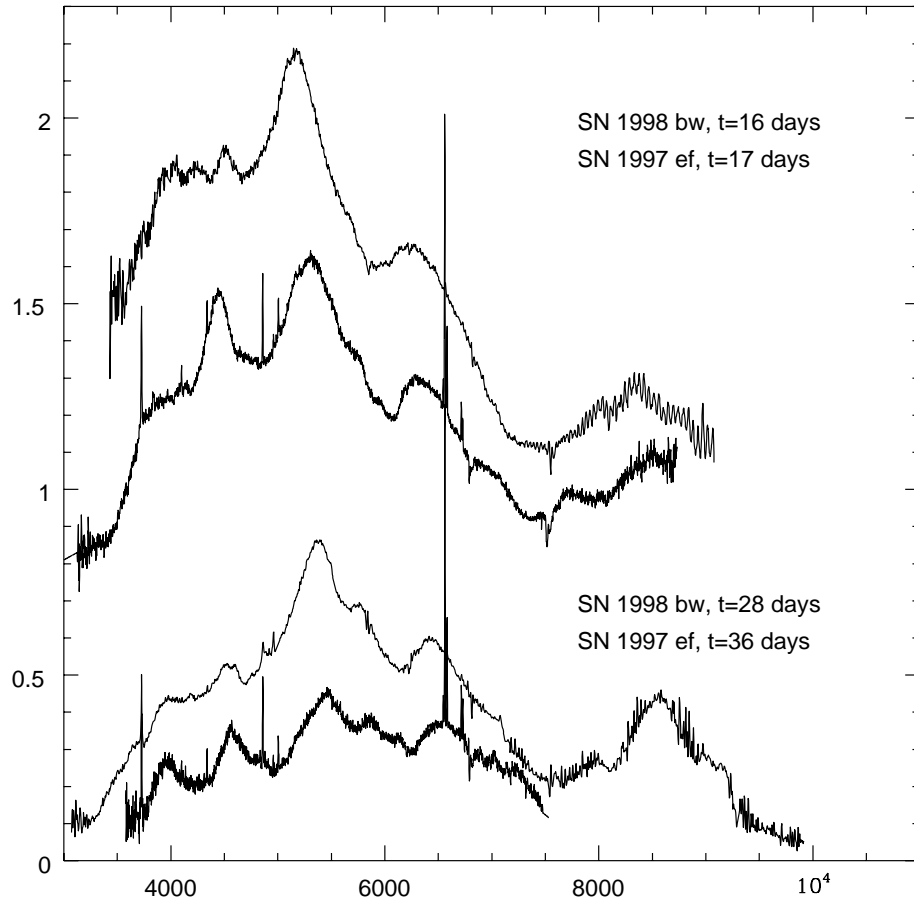


Fig. 1.— The observed spectra of Type Ic supernovae 1998bw (Iwamoto et al. 1998) and 1997ef.

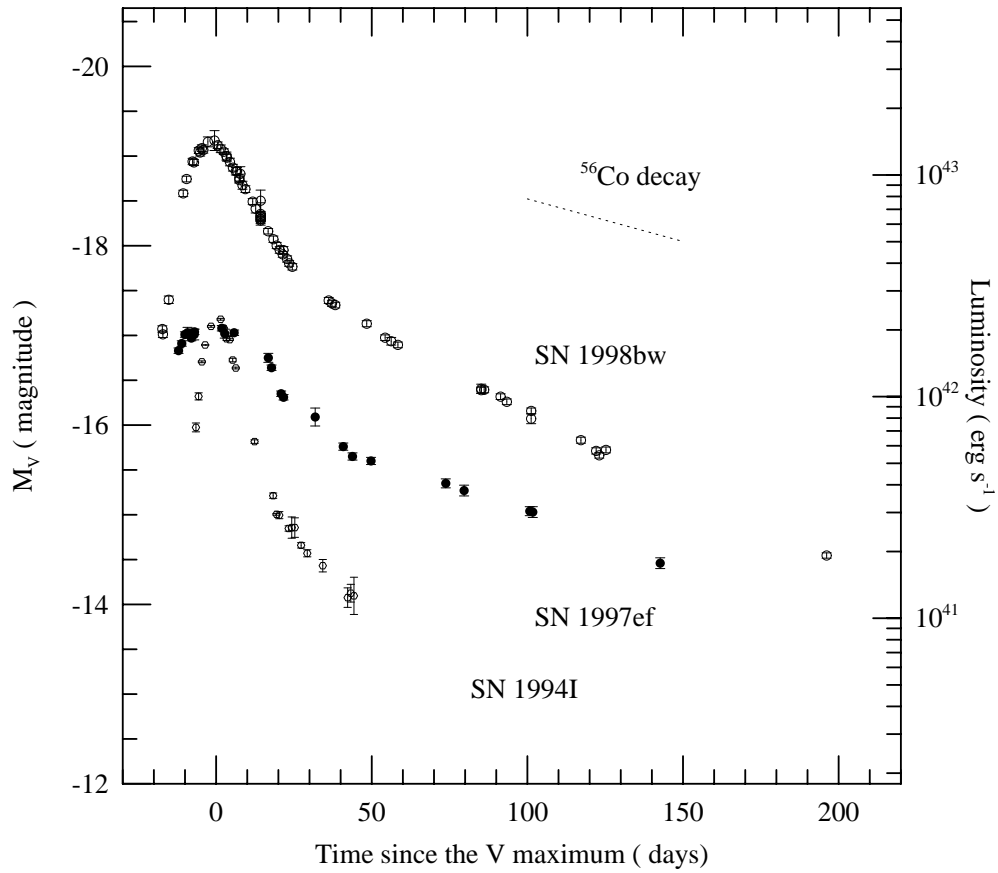


Fig. 2.— Absolute magnitudes of Type Ic supernovae: the ordinary SN Ic 1994I (Richmond et al. 1996a, b), the hypernova SN 1998bw (Galama et al. 1998), and the proposed hypernova SN 1997ef. The dashed line indicates the ⁵⁶Co decay rate.

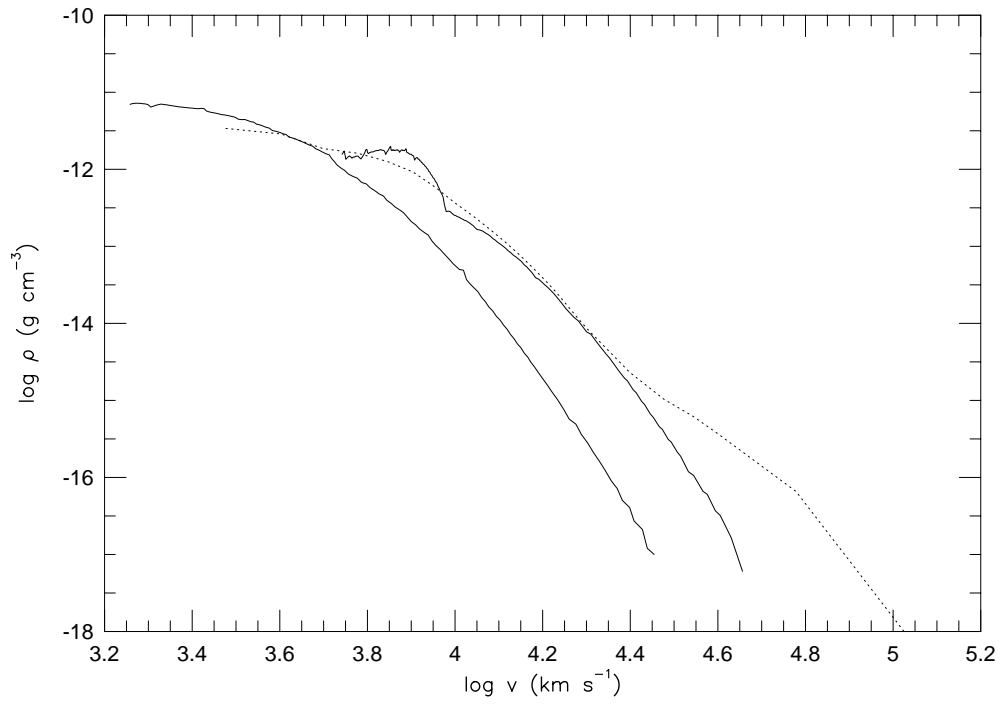


Fig. 3.— The density distributions against the velocity of homologously expanding ejecta for CO60 and CO100.

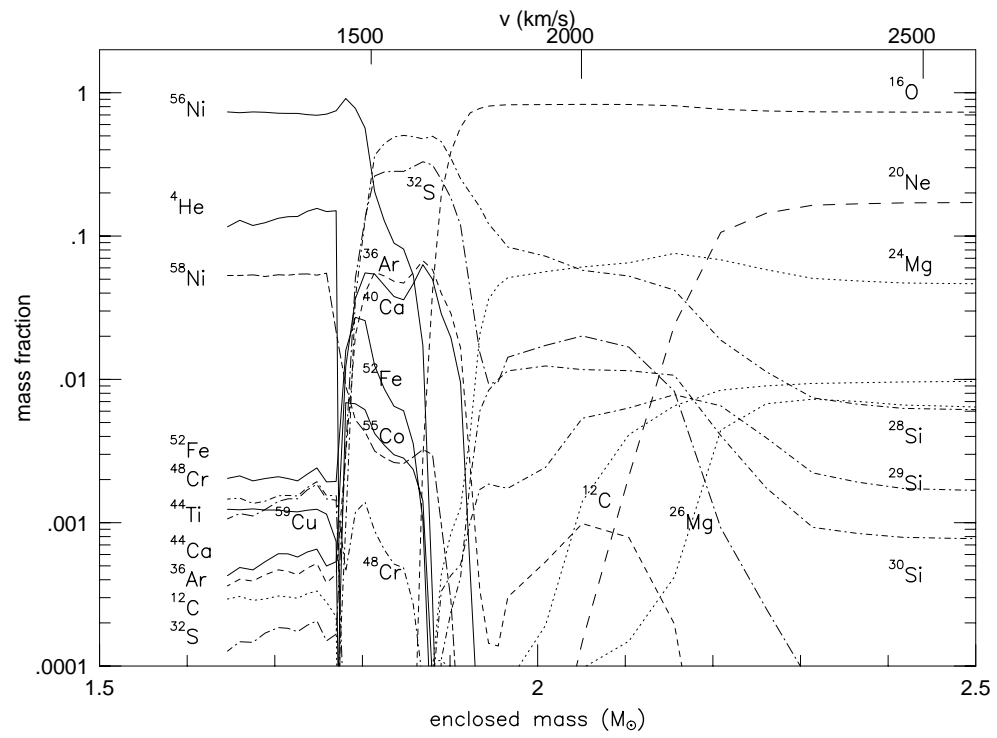


Fig. 4.— Chemical composition of model CO60 plotted against the expansion velocity.

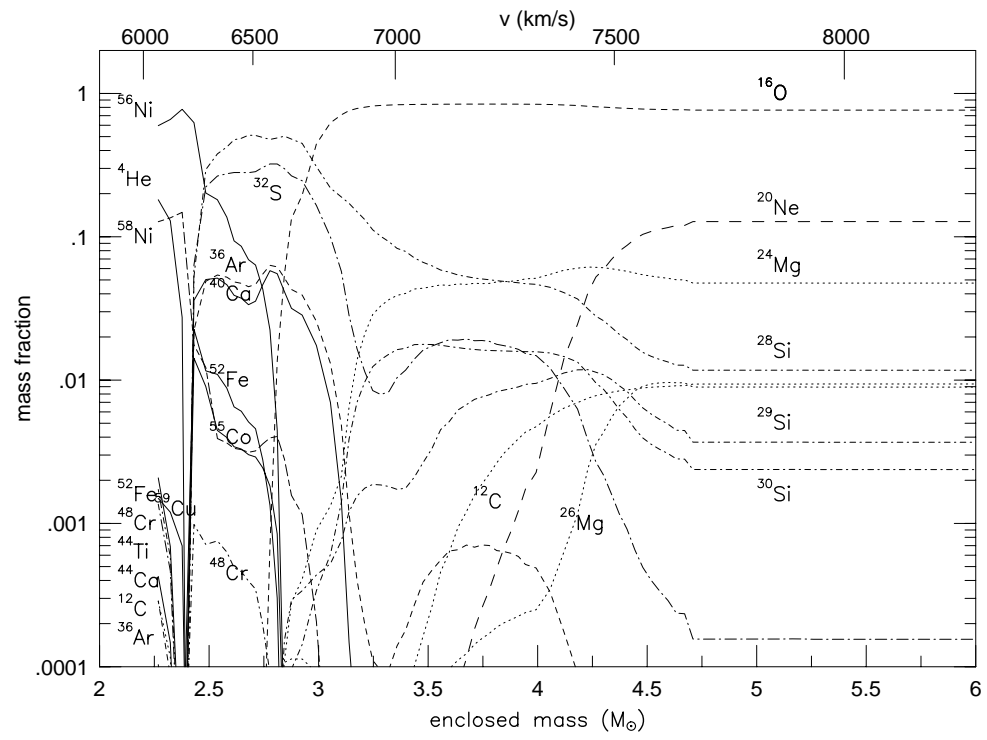


Fig. 5.— Chemical composition of model CO100 plotted against the expansion velocity.

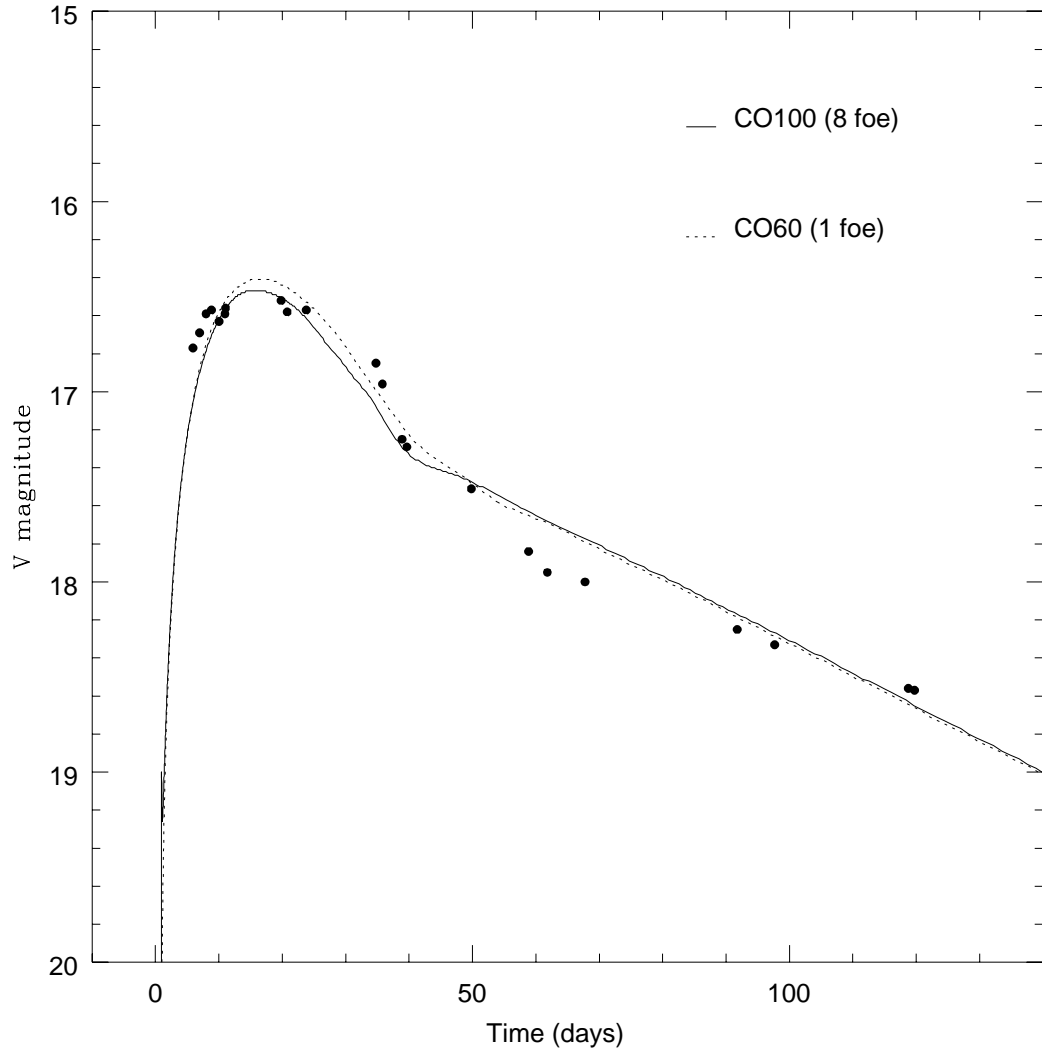


Fig. 6.— Calculated Visual light curves of CO60 and CO100 compared with that of SN 1997ef.

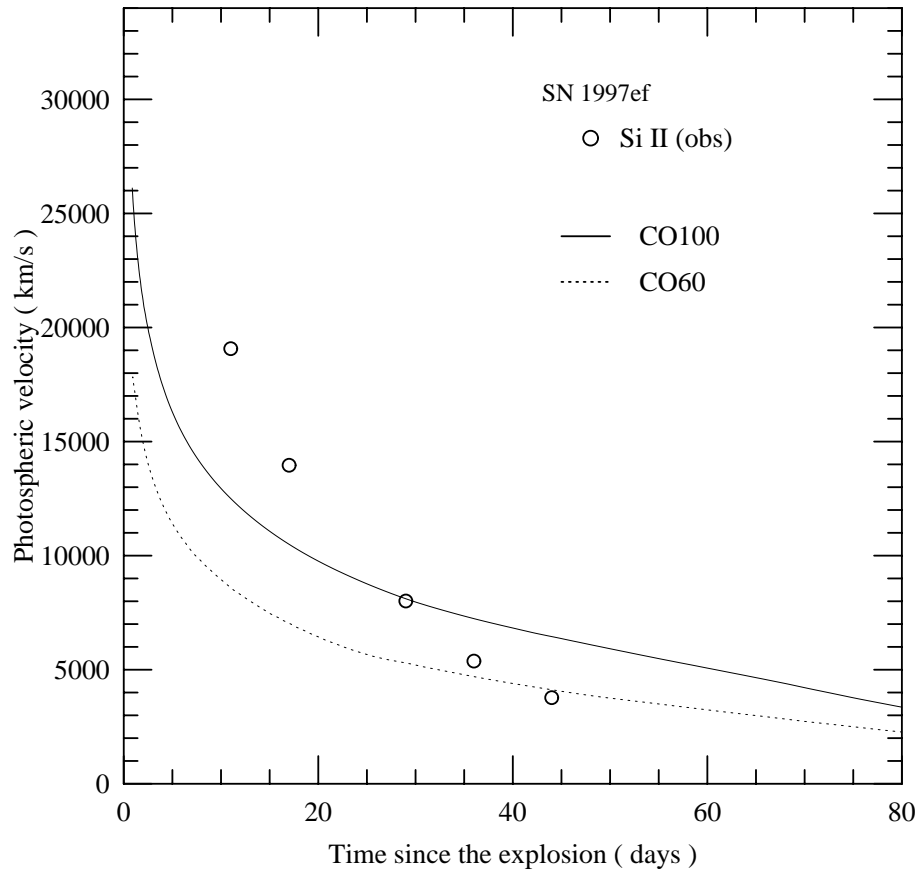


Fig. 7.— The evolution of the calculated photospheric velocities of CO60 and CO100 (solid lines) compared with the observed velocities of the Si II 634.7, 637.1 nm line measured in the spectra at the absorption core.

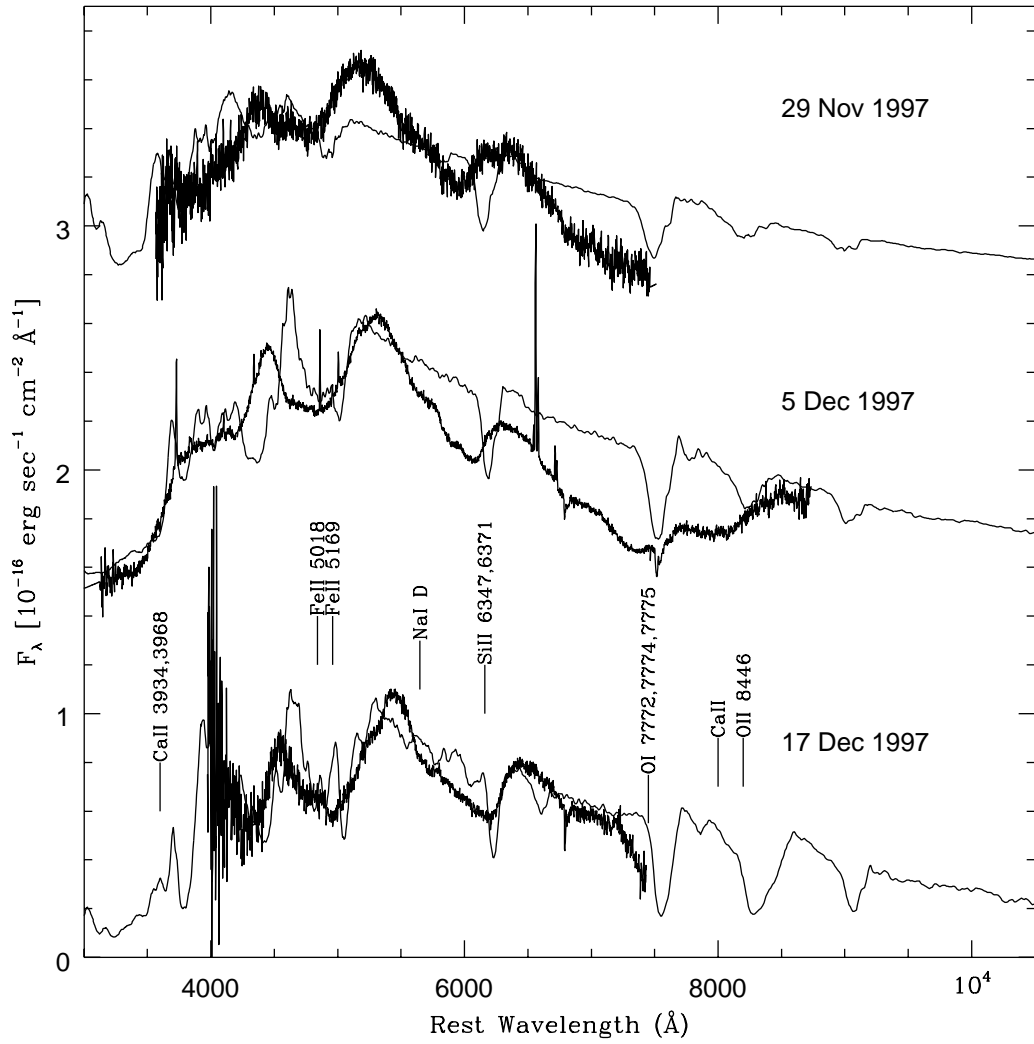


Fig. 8.— Observed spectra of SN 1997ef (bold lines) and synthetic spectra computed using model CO60. The lines in the synthetic spectra are much too narrow.

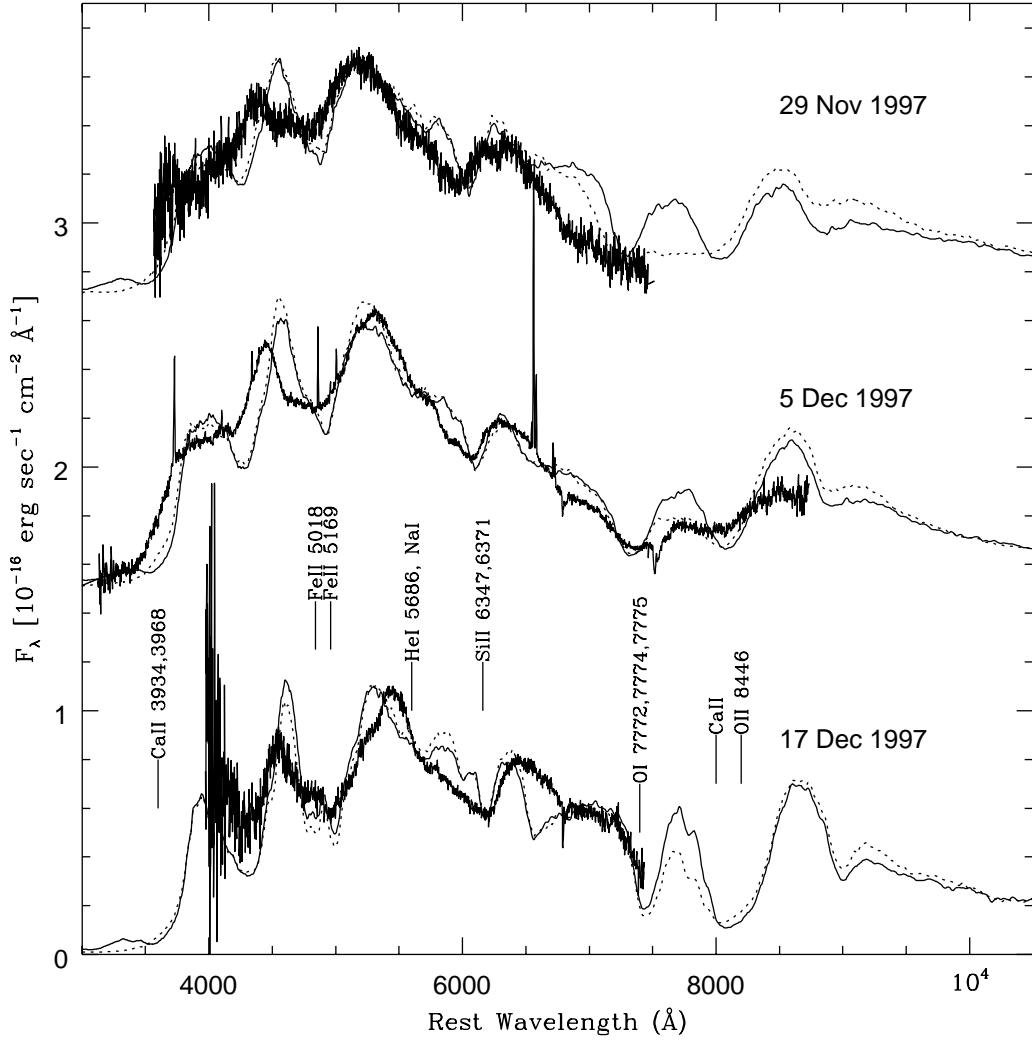


Fig. 9.— Comparison between the observed spectra of SN 1997ef and observed spectra of SN 1997ef (bold lines) and synthetic spectra computed using model CO100 (fully drawn lines) and for an arbitrary flattening of the density profile above $25,000 \text{ km s}^{-1}$. This change is necessary to reproduce the observed width of the Ca II IR triplet on Dec. 5.

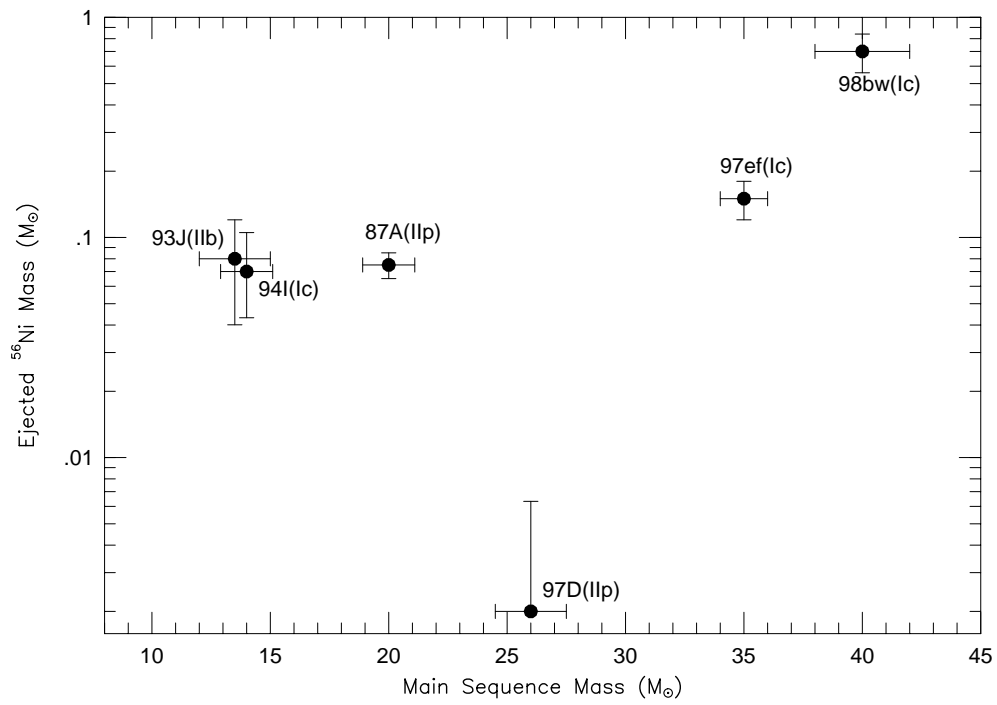


Fig. 10.— Ejected ^{56}Ni mass versus the main sequence mass of the progenitors of several bright supernovae obtained from light curve models.